UHV, Electrochemical NMR, and Electrochemical Studies of Platinum/Ruthenium Fuel Cell Catalysts

C. Lu, C. Rice, and R. I. Masel*

University of Illinois, Department of Chemical Engineering, Urbana, Illinois 61801

P. K. Babu, P. Waszczuk, H. S. Kim, E. Oldfield, and A. Wieckowski*

University of Illinois, Department of Chemistry, Urbana, Illinois 61801

Received: January 17, 2002; In Final Form: June 10, 2002

It is well-known that platinum/ruthenium fuel cell catalysts show enhanced CO tolerance compared to pure platinum electrodes, but the reasons are still being debated. We have combined cyclic voltammetry (CV), temperature programmed desorption (TPD), electrochemical nuclear magnetic resonance, and radio active labeling to probe the origin of the ruthenium enhancement in Pt electrodes modified through Ru deposition. The results prove that the addition of ruthenium not only modifies the electronic structure of all the platinum atoms but also leads to the creation of a new form of adsorbed CO. This new form of CO may be ascribed to CO chemisorbed onto the "Ru" region of the electrode surface. TPD and CV results show that the binding of hydrogen is substantially modified due to the presence of Ru. Surprisingly though, TPD indicates that the binding energy of CO on platinum is only weakly affected. Therefore, the changes in the bond energy of CO due to the ligand effect only play a small role in enhancing CO tolerance. Instead, we find that the main effect of ruthenium is to activate water to form OH. Quantitative estimates based on the TPD data indicate that the bifunctional mechanism is about four times larger than the ligand effect.

Introduction

Ruthenium addition is known to substantially enhance the CO tolerance of platinum fuel cell anodes. The increased CO tolerance allows fuel cells to run with reformates. It also enhances the rate of direct methanol electrooxidation. The origin of ruthenium enhancement is not completely understood. There are two widely accepted theories for the enhancement: the bifunctional mechanism[1−5] and the ligand model.[6−10] The bifunctional mechanism holds that the main effect of the ruthenium addition is to activate water molecules on the ruthenium surface to yield Ru−OH

$$Ru^0 + H_2O \rightarrow Ru\text{-}OH + e^- + H^+ \quad (1)$$

CO then migrates along the anode surface to react with the Ru−OH

$$Pt\text{-}CO + Ru\text{-}OH \rightarrow CO_2 + e^- + H^+ + Pt^0 + Ru^0 \quad (2)$$

Pure ruthenium forms surface hydroxides at lower potentials (>0.3 V vs RHE) than on platinum (0.6 V vs RHE),[3,6,11,12] so the removal of CO is much faster on a platinum/ruthenium surface than on pure platinum.

The Ligand model asserts that the main role of ruthenium is to modify the electronic structure of platinum surface by interacting with the conduction band of platinum. This modification is then presumed to induce a weakening of the Pt−CO bond, so that less energy is required to oxidize the adsorbed CO. Previous NMR investigation[13] of CO (generated from methanol) adsorbed on Pt electrode surfaces decorated with Ru has shown that there is a significant electronic alteration for platinum atoms near ruthenium islands. However, Pt atoms away from Ru are only weakly affected.

In this report, several surface techniques are combined to probe the role of ruthenium in improving the CO tolerance of platinum fuel cell catalysts. Cyclic voltammetry (CV) is used to determine how the kinetics of CO and hydrogen removal from the substrate change in the presence of ruthenium. Electrochemical nuclear magnetic resonance (EC NMR) is used to provide a measure of the electronic interactions between adsorbed CO (from CO saturated media) and the metal substrate. Radioactive labeling is used to measure the onset potential for CO oxidation. Temperature programmed desorption (TPD) is used to quantify the changes in binding energies of the various species, and the activation energy of surface hydroxide formation. A comparison is made between the measurements carried out on ruthenium modified Pt(110) single crystals and platinum nanoparticles.

Experimental Section

The TPD experiments were preformed on a Pt(110) single crystal, in a UHV chamber having a base pressure of 1×10^{-10} Torr. The apparatus and procedures have been described elsewhere.[14−17] The Pt (110) single crystal was cleaned by heating in oxygen at 800 °C and sputtering with argon ions, followed by annealing for 3 min at 1000 °C. Ru deposited on the single crystals through spontaneous deposition when used for UHV experiments always showed some carbon contamination that was difficult to remove. Therefore, chemical vapor deposition (CVD) was used to decorate the Pt single crystals

* To whom correspondence should be addressed.

10.1021/jp020169u CCC: $22.00
Published on Web 08/24/2002

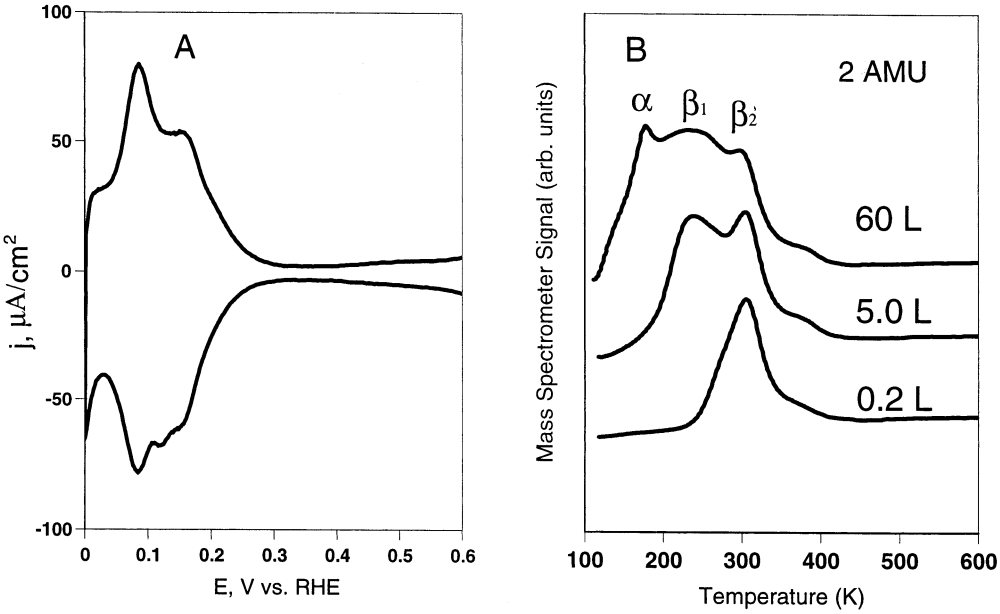

Figure 1. (A) Cyclic voltammogram of a clean Pt(110) electrode at a sweep rate of 50 mV s^{-1} in 0.1 M $HClO_4$ solution. Focusing on the hydrogen adsorption/desorption region. (B) A series of 2 amu TPD spectra taken by exposing a clean Pt(110) surface to various amounts of H_2 at 100 K and then heating at 15 K/s.

with Ru for carrying out the UHV experiments by heating the sample to 220 °C in the presence of 5×10^{-8} Torr of $Ru_3(CO)_{12}$. $Ru_3(CO)_{12}$ deposits a mixture of ruthenium and carbon, and so the carbon was removed by heating the sample to 300 °C in 2×10^{-7} Torr of oxygen for 30 min. The sample was then cooled to 100 K, and 5 Langmuirs (L) of hydrogen were added to reduce the surface oxide. Finally, the sample was flashed to 600 K to remove any residual hydrogen. A ruthenium coverage of 0.25 monolayers was obtained in this way. The sample was cooled to 110 K and dosed with hydrogen, CO, or water by backfilling the chamber. The TPD measurements were carried out at a heating rate of 15 K/s.

The Pt(110) single crystal used in the hydrogen adsorption/desorption electrochemical measurements was initially flame annealed and cooled in a nitrogen/hydrogen atmosphere. Spontaneous deposition of ruthenium was carried out at 0.3 V vs a RHE from $RuCl_3$ dissolved in 0.1 M $HClO_4$ to form 0.20 monolayers of Ru .[18] The cyclic voltammograms were acquired either in 0.1 M $HClO_4$ or in 0.1 M H_2SO_4 at a scan rate of 50 mV/sec.

Commercial fuel cell grade platinum black nanoparticles (Johnson Matthey) were modified by spontaneous deposition of ruthenium onto the platinum substrate to yield from 0.14 to 0.52 monolayers of ruthenium, as estimated by inductively coupled plasma spectroscopy. From scanning tunneling microscopy of Pt single crystals decorated by Ru through spontaneous deposition, we have found that Ru forms essentially monolayer islands of about 3−5 nm.[19] Though, there has not been any direct evidence of the form in which Ru is deposited on Pt nanoparticle electrode surfaces, we assume that the behavior is not different from that of Pt single-crystal surfaces. Electrochemical measurements were preformed on catalysts prepared by this technique. Current−time measurements of 0.5 M methanol electrooxidation in 0.5 M H_2SO_4 were carried out at 0.3 V vs RHE with the current levels reaching steady-state values within 10 h. Prior to the cyclic voltammetry measurements, methanol was chemisorbed onto the catalyst surface to form CO at 0.19V in 0.5 M H_2SO_4. After extended adsorption time (12 h) at low potentials, 0.9 monolayer CO coverage was attained. CO stripping was performed at a scan rate of 10 mV/min.

Technical details of the ^{13}C EC NMR measurements have been reported previously.[13,20] The Pt black based catalysts were prepared as above by spontaneous deposition of Ru and NMR samples were made from these catalysts as follows: CO was chemisorbed onto about 500 mg of catalyst from ^{13}C (99%) enriched CO solutions at an open circuit. After 1 h of adsorption, excess CO was removed by purging with argon and rinsing with 0.1 M D_2SO_4. The nanoparticles were then transferred into an NMR ampule containing a small (1−2 mL) portion of electrolyte and then flame sealed. Spectra and relaxation rates were obtained with a home-built solid-state NMR spectrometer, operated in 8.5 T magnetic field.

The radioactive labeling experiments[21] were done under potential control and slow scan-rate conditions, in a three-electrode electrochemical cell. The bottom of the cell was a radiation detector: a glass scintillation disk. The disk was covered with 7.5 μm thick polyimide film, onto which a 500 Å layer of gold was vacuum deposited. The working electrode was prepared by placing platinum black or ruthenium decorated Pt nanoparticles on top of the gold conducting support. CO is adsorbed onto the surface from 0.01 M methanol and 0.1 M H_2SO_4 solution at 0.2 V vs a standard hydrogen reference electrode.

Results: Adsorption/Desorption Studies

Hydrogen Desorption. Figure 1A,B compares the CV and TPD spectra of hydrogen desorption from Pt(110). The CV shows that hydrogen desorbs in two peaks at 0.086 and 0.150 V. The adsorption part of the CV consists of a peak at 0.084 V and a sideband between 0.150 and 0.20 V (Figure 1A), in addition to a peak near 0 V, associated with H_2 evolution. These data were taken in perchloric acid. When the same measurements were done in sulfuric acid, the 0.150 V band moves to 0.160 V and the 0.086 V band is suppressed due to interaction with the sulfate ions.

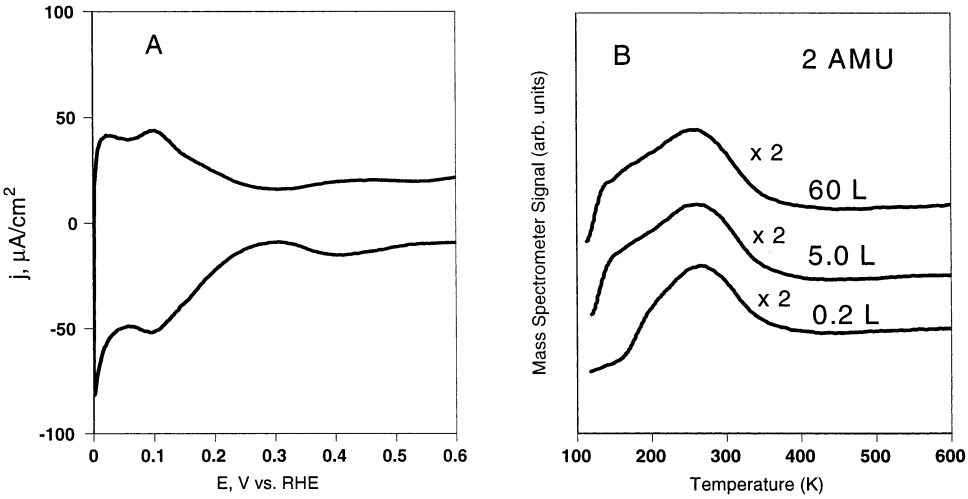

Figure 2. (A) Cyclic voltammogram of a Pt(110)/Ru electrode (obtained through spontaneous deposition) at a sweep rate of 50 mV s^{-1} in 0.1 M $HClO_4$ solution. (B) A series of 2 amu TPD spectra taken by exposing Pt(110)/Ru (obtained through CVD) to various amounts of H_2 at 100 K and then heating at 15 K/s. At low exposures the hydrogen coverage is less that a full monolayer, while the coverage at the maximum exposure time is in slight excess of a full monolayer.

At coverages below $^1/_2$ of saturation, the TPD spectrum shows a single peak, commonly called the β_2 peak, at 300 K (Figure 1B).[17] At higher coverages, a second peak, called the β_1 peak grows into the spectrum at 270 K.[17] The β_1 peak shifts to 230 K with increasing coverage. At coverages above 40% of saturation, an additional peak commonly called the α peak is seen at 180 K.[17]

Figure 2A,B shows cyclic voltammogram and TPD spectra on ruthenium modified Pt(110) samples. The CV spectrum shows a hydrogen desorption peak at 0.102 V and an adsorption feature at 0.092 V (Figure 2A). There is also a hydrogen desorption feature at 0.040 V and an H_2 evolution feature at 0.0 V. A comparison of Figures 1A and 2A shows that the addition of a quarter of a monolayer ruthenium decreases the primary hydrogen desorption potential by about 10 mV. The secondary desorption peak observed on the clean platinum surface disappears with the addition of a quarter of a monolayer ruthenium. The peaks are also broadened due to the increase in surface heterogeneity. There is also a 30% decrease in the amount of hydrogen adsorbed.

Figure 2B shows a series of TPD spectra for hydrogen desorption from a ruthenium modified Pt(110) surface. Peaks are seen at 140∼170 K and at 260 K. The peaks are broader than that on the clean surface, similar to the behavior observed for CV. The total amount of hydrogen adsorption decreases to a little less than one-half when ruthenium is present on the surface. A comparison of Figures 1B and 2B shows that the binding of hydrogen is substantially modified by the presence of ruthenium, proving that ruthenium has a significant effect on the properties of platinum, even though pure ruthenium binds hydrogen strongly.[27]

CO Binding. Figure 3A,B represents CO peaks on pure platinum black probed via CO stripping CV and CO desorption TPD. In Figure 3A, CO was adsorbed onto platinum black nanoparticles to form 0.9 monolayers. CO is then removed from the surface by slowly scanning the potential (10 mV/min). As the potential becomes more anodic, water is activated on the platinum surface, and CO is oxidized by, for example, the following reaction

$$\text{Pt-CO} + \text{Pt-OH} \rightarrow CO_2 + 2Pt^0 + e^- + H^+ \qquad (3)$$

Figure 3A shows only one CO stripping peak at 0.522 V. Figure 3B shows a series of TPD spectra for CO desorption from Pt(110). At moderate coverages, only one peak is present at 515 K. At higher CO coverages, a second peak begins to form at 415 K.

^{13}C EC NMR spectrum of chemisorbed CO from the CO saturated solution on platinum black nanoparticles in 0.1 M H_2SO_4 is shown in Figure 4A. A single resonance peak at 369 ppm is found as before in experiments where CO was generated from methanol. For comparison, the ^{13}C NMR spectrum of CO adsorbed via methanol oxidation is given in Figure 4B. Because about 500 mg of Pt nanoparticles are required for the NMR sample preparation, methanol oxidation is found to produce CO coverages in the region 0.7−0.8 monolayers only. On the other hand, when CO is adsorbed from CO saturated solution, surface coverage of about 0.9 monolayers can be achieved. The slight increase in the width of the NMR spectrum for the CO chemisorbed from the gas-phase arises due to the increased dipolar interaction between the CO molecules as a consequence of the higher CO coverage. The relaxation rates and their temperature variation (see Table 1) are found to be identical for both the cases, implying that CO adsorbed on Pt has the same electronic properties irrespective of its source of generation.

Figure 5 shows how the presence of ruthenium alters the CO stripping CV, TPD spectrum for CO desorption and ^{13}C NMR spectrum of adsorbed CO. Two CO stripping peaks are obtained from slow scan cyclic voltammetry (10 mV/min) on ruthenium modified platinum nanoparticles at 0.407 and 0.30 V (Figure 5A), corresponding to CO bound to platinum and ruthenium. There are also two peaks at around 480 and 400 K in TPD (Figure 5B), and two peaks at 359 and 159 ppm can be obtained through standard deconvolution of the ^{13}C NMR spectrum (Figure 5C). A comparison of these results to those in Figures 3 and 4 show that there are two key effects due to ruthenium addition: (i) a small shift in the peak positions for all of the spectra and (ii) formation of a weakly bound form of CO that can be associated with CO adsorbed on or near Ru islands.

It is interesting to quantify these two key effects due to the presence of Ru. An Arrhenius plot on the initial part of the TPD curves shows a 2 kcal/mol decrease in the binding energy of CO compared to the clean surface. There is also a 10 ppm shift in the ^{13}C NMR of CO bound to Pt atoms away from Ru islands (remote Pt). Thus, it appears that all the CO molecules

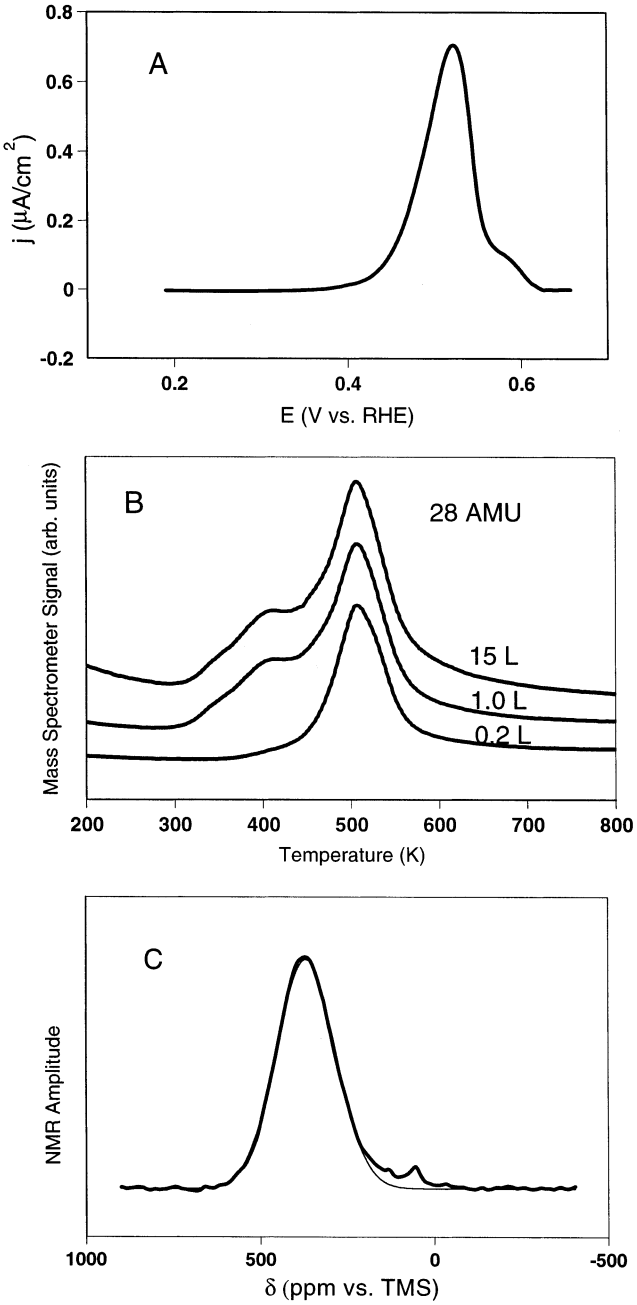

Figure 3. (A) CO stripping voltammogram on Pt black nanoparticles, at a slow scan rate of 10 mV/min in 0.5 M H_2SO_4, after 12 h of methanol oxidation to form CO at 0.19 V vs RHE. (B) A series of 28 amu TPD spectra taken by exposing Pt(110) to various amounts of CO at 100 K and then heating at 15 K/s.

bound to platinum are affected by ruthenium. However, the effect is smaller than that found in the hydrogen TPD spectra in Figure 2. Evidently, ruthenium is not changing the binding of CO to remote Pt to a great extent, even though there is a substantial effect on the binding of hydrogen.

For the weakly bound form of CO, TPD shows that a peak appears at 400 K for the ruthenium covered electrode surfaces. The peak in the NMR spectrum corresponding to this CO has a smaller Knight shift, proving that this CO has a weaker interaction with the metal surface than those on the clean surface. From the CO stripping CV, it is clear that the CO adsorbed on the Ru phase is easier to oxidize than the CO on Pt phase of the Pt/Ru electrode. However, the former peak is not important

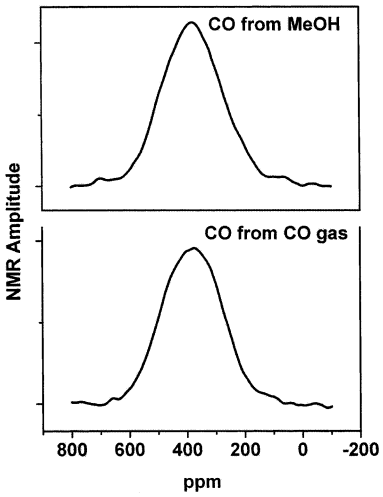

Figure 4. (A) ^{13}C NMR spectrum of chemisorbed CO from the CO saturated solution on Pt-black nanoparticles. (B) ^{13}C NMR spectrum of chemisorbed CO on Pt-black from methanol oxidation.

TABLE 1: Comparison of the ^{13}C NMR Spectrum of CO Produced from CO and Methanol on a Nanocrystalline Platinum Catalyst.

	CO (from MeOH)	CO (from CO gas)
peak (ppm)	369	369
T_1T (s.K)	59	57
$D_{5\sigma}(E_f)$ (Ry.atom)$^{-1}$	0.6	0.6
$D_{2\pi^*}(E_f)$ (Ry.atom)$^{-1}$	7.0	7.3

in a fuel cell because CO from the Ru phase is oxidized at potentials at or below those typically used in a fuel cell.

Figure 6 shows how the CO coverage varies with exposure, during CO adsorption on Pt(110) single crystals in UHV. On the clean surface, there is an initial rapid rise in the coverage, and then the coverage levels off. Similar behavior is seen on the ruthenium modified Pt(110) sample except that the saturation coverage is less than half of that on the clean surface. Interestingly, the initial parts of the curves are identical on the two samples suggesting that again the sticking probability is identical on the two samples.

Figure 7A,B illustrates the effect of ruthenium on the back-bonding of CO (adsorbed from CO saturated solutions) as measured by ^{13}C NMR. A single NMR peak is seen on the clean platinum surface at 369 ppm (Figure 7A). As the coverage of ruthenium is increased a second peak begins to emerge near 150 ppm.[13] Observation of two peaks for the NMR spectra is consistent with the two peaks found for the CO stripping CV of Ru covered Pt electrode surfaces. Therefore, we can ascribe the two-peak structure observed for CV and NMR to the same origin viz., formation of two different forms of adsorbed CO. Thus, for the deconvolution of the ^{13}C NMR spectra, we kept the ratio of the areas of the two peaks obtained from the CV, as a constraint. Relaxation measurements were carried out at these two peak positions to estimate the Fermi level local density of states (E_f-LDOS). The 150 ppm peak continues to grow with subsequent increase in the amount of deposited Ru, whereas the high field peak shift decreases from 370 to 350 ppm. Using the two-band models developed earlier and the correlations between ^{13}C chemical shift and the clean metal surface E_f-LDOS,[20] it was possible to obtain the $2\pi^*$ E_f-LDOS at the orbital of chemisorbed CO as well as that the total E_f-LDOS at the clean metal surface. Variation of these E_f-LDOS values with Ru coverage are shown in Figure 7B. For the weakly bound form of CO, there is about 70% reduction in the metal surface E_f-LDOS and about 30% reduction in the $2\pi^*$ E_f-LDOS (open

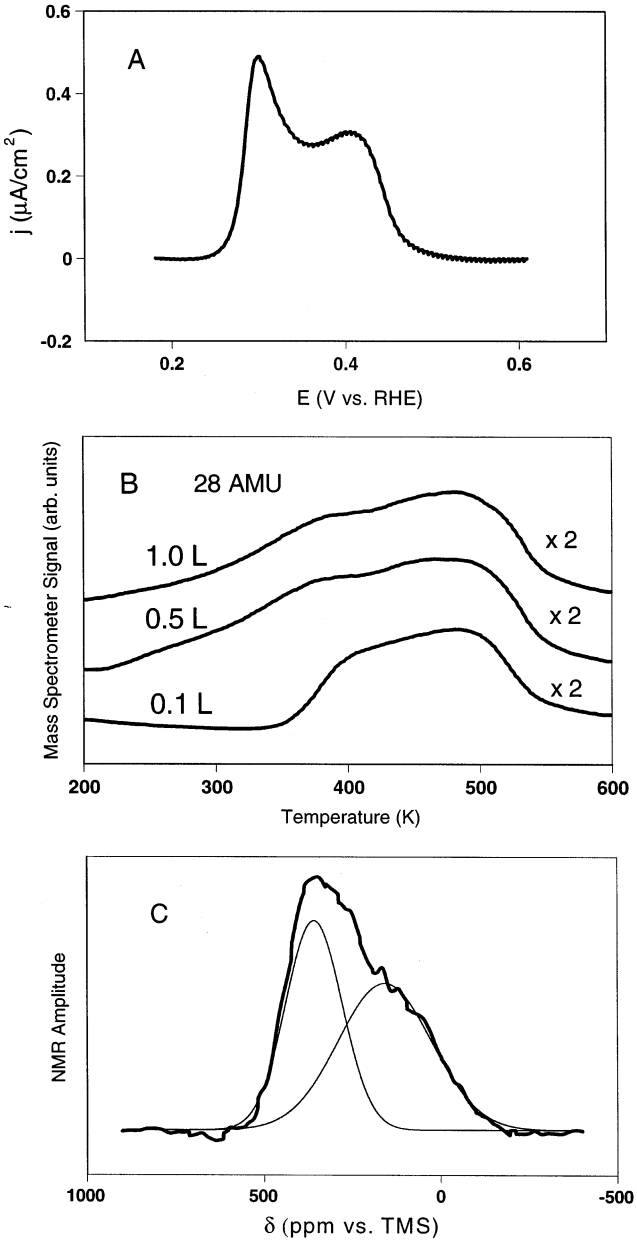

Figure 5. (A) CO stripping voltammogram on Ru modified Pt black nanoparticles (0.35 monolayers of Ru), at a slow scan rate of 10 mV/min in 0.5 M H_2SO_4, after 12 h of methanol oxidation to form CO at 0.19 V vs RHE. (B) A series of 28 amu TPD spectra taken by exposing Pt(110)/Ru (0.25 monolayers of Ru) to various amounts of CO at 100 K and then heating at 15K/s. (C) Spin−echo mapped ^{13}C EC NMR spectra of chemisorbed ^{13}C labeled CO on Ru modified Pt black nanoparticles (0.35 monolayers of Ru) in 0.5 M H_2SO_4, formed from 12 h methanol oxidation at 0.19 V vs RHE.

symbols in Figure 7B). However, for Pt atoms away from Ru, the changes in E_f-LDOS are comparatively less.

Results: Kinetic Measurements

Current−Time Transients. Next, we wish to examine the effect of ruthenium on the kinetics of methanol oxidation on platinum anodes. Figure 8 compares the methanol electrooxidation activity on platinum black nanoparticles modified with various amounts of Ru. On pure platinum nanoparticles, the methanol electrooxidation current at 0.3 V vs RHE decays immediately, due to CO passivation. In contrast, significant currents are observed on the ruthenium modified surfaces. The steady-state methanol oxidation current density also varies with

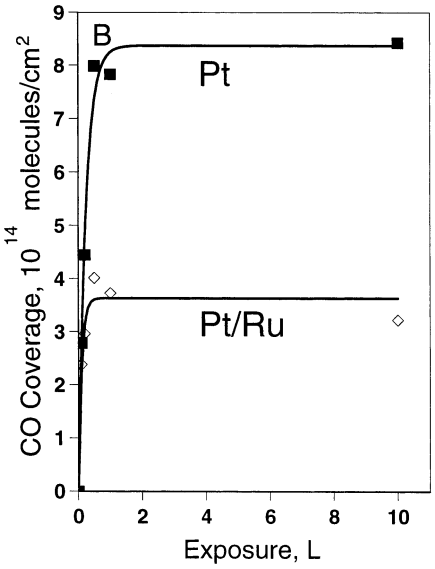

Figure 6. Comparison of CO adsorption kinetics on Pt(110) and Pt(110)/Ru vs exposure time by TPD methods. The coverages are calculated from integration of the TPD peak area normalized to the saturation coverage.

ruthenium content. A maximum enhancement in oxidation current by a factor of about 20 over that on pure platinum is found for the catalyst with 0.35 monolayers of Ru (Figure 8). The catalytic activity appears to level off at ca. 0.5 monolayers of ruthenium and a decrease in activity is observed for higher ruthenium coverages.[22]

TPD of ^{18}O. At this point, we have shown that there is about a 0.2 V decrease in the electro-catalytic potential to oxidize the strongly bound CO from the platinum surface, but TPD and NMR results show that the binding of strongly bound CO on platinum is only moderately affected by ruthenium. Therefore, we need to consider how ruthenium is making it easier to oxidize the CO when it is not strongly affecting its binding. One possibility is that ruthenium is activating water or hydroxyl on the surface which can increase the CO oxidation rate which is commonly referred to as the bifunctional mechanism. Figure 9 shows TPD results involving hydroxyls on Pt(110) and Pt(110)/Ru surfaces from ref 17. $^{18}O_2$ is adsorbed on the surface before normal $H_2 16O$ is added. Mass 20 amu spectrum shows two peaks at 160 and 205 K. The peak at lower temperature results from the ^{18}O exchange process through OH as the intermediate[23]

$$^{18}O + H_2O \rightarrow {}^{18}OH + OH \quad (4)$$

$$^{18}OH + OH \rightarrow H_2 18O + O \quad (5)$$

This reaction is water desorption rate limited.[24] The second peak involves hydroxyl formation and recombination. Oxygen reacting with hydrogen in the background yields hydroxyls, which then recombine to produce water.[23] This peak shows up by itself when water is not present. On Pt(110)/Ru surface, similar experiments are done with twice the amount of water dosage which gives approximately the same amount of adsorbed water as in the case of clean platinum surface. Only one peak at 160 K appears whose area is even larger than the sum of the two peaks on Pt(110). This indicates that the peak at 205 K on Pt(110) is now shifted below 160 K and the process of ^{18}O exchanging into water is enhanced. These results prove that

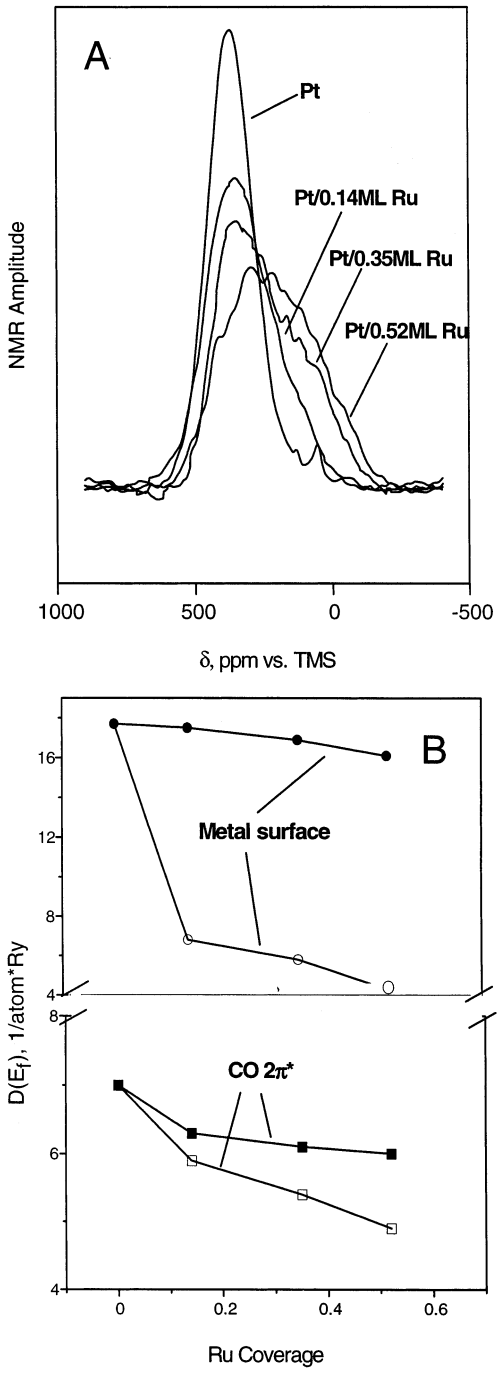

Figure 7. (A) Spin−echo mapped ^{13}C EC NMR spectra of chemisorbed ^{13}C labeled CO on Ru modified Pt black nanoparticles in 0.5 M H_2SO_4. Ru coverages correspond to 0.00, 0.14, 0.35, and 0.52 monolayers. (B) The metal surface E_f-LDOS was calculated from the ^{13}C NMR chemical shift for the strongly bound CO (open symbols) and the weakly bound CO (closed symbols). For chemisorbed ^{13}CO, $2\pi^*$ E_f-LDOS variation is shown for strongly bound (solid symbols) and weakly bound (open symbols) forms as a function of the Ru coverage.

water is much more active on a ruthenium modified Pt(110) surface than on clean platinum.

Discussion: Adsorption

Conceptually, electrochemical and thermal activation causing electrooxidation of chemisorbed species may be basically different. The difference may arise because two hydrogen atoms need to recombine to a H_2 molecule before desorbing to UHV, whereas atomic hydrogen is ionized to proton to leave the

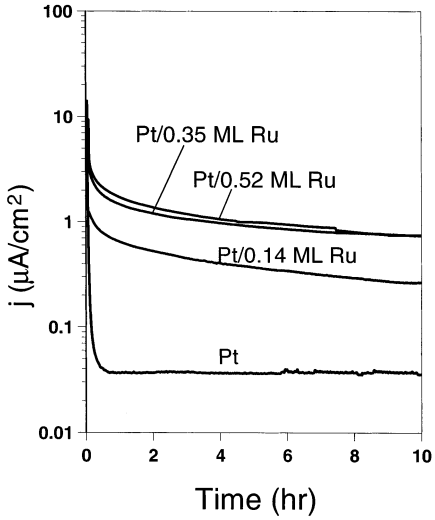

Figure 8. Current−time transients at 0.3 V vs RHE on both pure Pt black and Ru modified Pt black electrodes in 0.5 M methanol solution. The Ru coverage was varied; 0.00, 0.14, 0.35, and 0.52 monolayers of Ru.

electrode surface. However, clear similarities between voltammetry and TPD were found in this work, showing that the desorption is controlled through steps preceding both the recombination or hydrogen atom ionization. The hydrogen desorption peak as proton, seen at 0.15 V in CV, and the desorption peak as a H_2 molecule, observed at 300 K in TPD (Figure 1) are absent on the ruthenium modified surface. Ruthenium deposition on Pt(110) is reducing the hydrogen coverage and binding energy of hydrogen both in an electrochemical cell and UHV. This contributes to simplification of the fine structure of the CV curves and TPD spectra (Figure 2, cf. with Figure 1). There is, therefore, a clear correspondence between the data obtained in these two dissimilar environments. On this basis, we may interpret the data from UHV and electrochemical cell jointly.

The results in this investigation provide a consistent picture about the effects of ruthenium on hydrogen and CO adsorption and oxidation on platinum. First, the data show a strong modification in the electronic structure of platinum when ruthenium is added. Hydrogen TPD reveals that the strongly bound state of H_2 at 300 K disappears. CV shows that one hydrogen desorption peak at higher potential (0.16 V) disappears. NMR data reveal that the E_f-LDOS of all the adsorbed CO decreases with increasing ruthenium coverage. The H_2 peak seen at 0.15 V in CV, and 300 K in TPD (Figure 1) are absent on the ruthenium modified surface. If some of the platinum atoms were unaffected by ruthenium, one would expect to see these peaks on the ruthenium modified surface too, but Figure 2 shows no evidence for that. Therefore, addition of ruthenium modifies the electronic structure of the entire platinum surface.

Surprisingly, the changes in the electronic structure of platinum have only a mild effect on the binding energy of CO. TPD shows that the desorption temperatures of CO on Pt(110)/Ru are about 400 and 480 K, compared to 415 and 515 K on a clean Pt(110) surface. This corresponds to a change of about 2 kcal/mol in the binding energy of CO. The NMR peak of strongly bound CO shifts by only 10−20 ppm. By comparison, hydrogen TPD shows a 100 K change in desorption temperature. These observations suggest that the binding of strongly bound CO is only marginally affected by ruthenium, even though the hydrogen TPD and CV data prove that the whole surface is

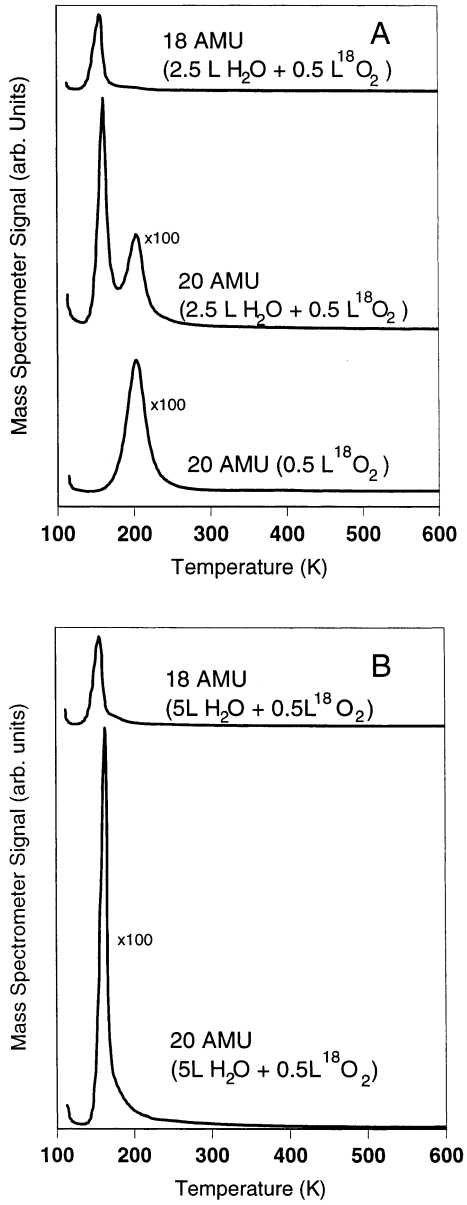

Figure 9. (A) 18 and 20 amu TPD spectra taken by adsorbing about 0.5×10^{15} molecules/cm^2 of ^{18}O then adding about 1×10^{15} molecules/cm^2 of $H_2$16O onto Pt(110) before flashing in a background containing 1×10^{-10} Torr of hydrogen with a rate of 15 K/s. (B) Repeat the same experiment as in A on Pt(110)/Ru

being affected by ruthenium. The TPD experiments in Figure 6 confirm that the initial CO adsorption is unaffected by the presence of Ru, suggesting a similarity in sticking probability on both Pt and Pt/Ru surfaces at the beginning of the process. As the surface population of CO grows, the adsorption rate decreases.

Discussion: Kinetics Measurements

Next, we wish to focus on the role of ruthenium in promoting CO oxidation from the platinum surface. Recall that previous investigators[1−7,9−12,25] have found that platinum−ruthenium catalysts are much more CO tolerant than pure platinum catalysts. It is thought that the main mode of CO oxidation is a simple process:

$$\text{M-CO} + \text{M-OH} \rightarrow CO_2 + 2\text{M} + e^- + H^+ \qquad (6)$$

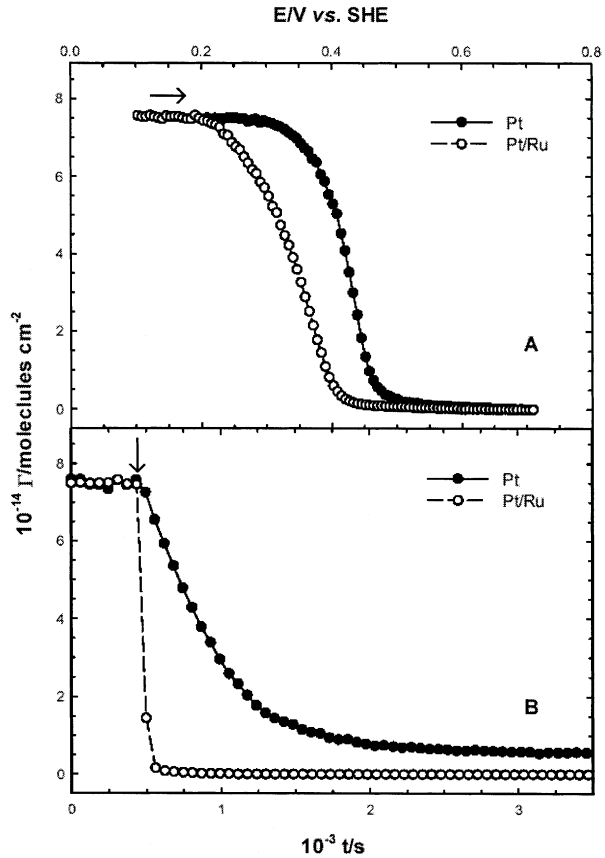

Figure 10. (A) Comparison of CO desorption kinetics at Pt Black and Ru decorated Pt nanoparticle catalysts using radioactive labeling and the slow-scan, positive-going electrode polarization. Catalyst loading is 0.4 mg cm^{-2}. (B) Comparison of CO desorption kinetics (also to the clean electrolyte) at Pt Black and Pt/Ru decorated nanoparticle catalyst using radioactive labeling and potential step experiment, from 0.1 to 0.43 V. (The arrow indicates the potential step.)

Under some conditions, the CO might also desorb from the platinum surface, especially at low potentials and high temperature.[26]

Figure 10A compares radioactive labeling data of ^{14}CO oxidation on platinum black and the platinum/ruthenium electrode obtained under slow-scan polarization conditions. CO was formed on the catalyst surface from 0.01 M methanol (^{14}C labeled) in 0.1 M H_2SO_4 at 0.1 V vs SHE. Once a constant CO coverage, corresponding to surface concentration of 7.5×10^{14} molecules cm^{-2} was obtained, methanol was washed off from the solution, the surface concentration was re-checked, and the positive-going scan of 0.1 mV/s was applied. The data show that within most of the hydrogen region, there is no CO oxidation from the surface, and neither is there any significant change in the coverage between pure Pt and Ru decorated Pt. The CO oxidation does not begin until 0.3 V on platinum black, as seen by the drop in count rates (Figure 10A). However, on platinum/ruthenium the CO oxidation is initiated at 0.1 V more negative potential showing that there is about a 0.1 V reduction in the energy to oxidize CO from the Pt/Ru surface. The Γ vs E branch is negatively shifted with the deposited Ru coverage up to the maximum value of 0.2 V, confirming data in the previous study.[21] Similar separations were observed on the Pt(111) electrode decorated by ruthenium regardless of whether the CO adlayer was created from methanol or a gaseous CO precursor.

Further support for the strong effect of surface ruthenium on the CO oxidation process is provided by the data in Figure 10B.

The beginning of the experiment was the same as reported above, and the constant surface concentration of CO was measured at 0.1V vs SHE in the clean supporting acid electrolyte. Next, instead of applying the slow-scan polarization, the potential was stepped to 0.43 V. It is shown in Figure 10B that the oxidative CO desorption is much faster on Pt/Ru than on Pt, and that the process is incomplete on pure platinum. Clearly, there exists a significant difference in the stability of CO on these two surfaces. Thus, the data in Figure 10 also show that platinum/ruthenium is much more CO tolerant than pure platinum.

Finally, we can use the TPD data to quantify the contributions of the ligand effect and the bifunctional mechanism on the enhancement of reaction 6. TPD results yield only about 2 kcal/mol reduction in the binding energy of strongly bound CO and ^{13}C NMR shows a maximum of 20 ppm peak shift for strongly bound CO. According to the Polanyi relationship[27] a 2 kcal change in the binding energy of the CO on the rate should only produce about a 40 mV reduction in the activation barrier for reaction 6.[17] That is insufficient to explain the 200 mV reduction in potential observed in Figure 10. Therefore, the ligand effect alone is insufficient to explain the reduction in the potential for CO oxidation. However, although the ligand effect is overall small, there is clear evidence from XAS[28] and NMR[13] data that there is a sharing of electrons between platinum and ruthenium. This sharing of electrons reduces the $2\pi^*$ E_f-LDOS on the C−O bond in the CO chemisorbed state on Pt/Ru electrodes.

As explained earlier, the data in Figure 9 show that an additional role of ruthenium is to activate water. One can make a quantitative estimate of this effect by comparing the activation barrier for OH recombination on a clean surface to that on a ruthenium covered one. Assuming a preexponential factor of 10^{13}/sec, we have calculated an activation barrier of 12 kcal/mol for OH recombination on the clean surface. It is harder to get an accurate value on a ruthenium covered surface. The OH recombination peak is at 160 K on the ruthenium covered surface. Water itself desorbs at 160 K, so the 160 K peak must be desorption limited but not reaction limited. Therefore, one cannot use TPD to accurately measure the activation barrier for OH recombination on the ruthenium covered surface. Still, the barrier for OH recombination on the ruthenium covered surface must be less than the activation barrier for desorption of water, 9 kcal/mol, because water desorption is rate determining. Further, the barrier for OH recombination on the ruthenium covered surface must be at least 7 kcal/mol or else we would have observed water formation during dosing at 100 K. Thus, the presence of ruthenium has reduced the barrier for OH recombination from 12 kcal/mol to 7−9 kcal/mol.[17] This result shows that the bifunctional mechanism is active on the ruthenium covered platinum surface producing a 3−5 kcal/mol reduction in the activation barrier for hydroxyl recombination. According to the Polanyi relationship, a 3−5 kcal/mol reduction in the activation barrier for hydroxyl recombination should translate into a 130 to 220 mV reduction in the activation barrier to oxidize CO.

Notice that the total reduction in the potential for CO oxidation inferred from TPD (170 to 260 mV) agree quite well with the 200 mV reduction observed in ref 22 and in this study at high Ru coverage. Consequently, it does appear that the TPD measurements are reproducing the changes seen in the electrochemical experiment. From the TPD data, we can conclude that although both the "ligand model" and the "bifunctional mechanism" seem to be active on our sample the bifunctional effects seem to be larger than the ligand effects. According to our data, of the 4−6 kcal/mol (170−260 meV) reduction in the potential for CO oxidation, only about 1 kcal/mol (40 meV) is associated with the ligand effect, whereas 3−5 kcal/mol (130 to 200 meV) are associated with the bifunctional mechanism. Thus, the effect of the bifunctional mechanism is about 4 times larger than the ligand effect.

Conclusions

This investigation explored the effect of ruthenium on the CO tolerance of platinum fuel cell anodes. We find that ruthenium has a major effect on the electronic structure of platinum. The E_f-LDOS of ^{13}CO at Pt sites near Ru decreases substantially while the binding energy of H_2 shows a significant drop. CO oxidation occurs at a potential 200 mV lower on platinum/ruthenium than on platinum. Surprisingly, ruthenium only has a small effect on the binding of CO to platinum atoms that are away from Ru. The initial sticking probabilities are identical for platinum and platinum/ruthenium surfaces. TPD indicates that the binding energy of the strongly bound form of CO is changed by only 2 kcal/mol and the NMR peaks shift by only 10−20 ppm.[13]

Analysis of our TPD data indicates that, of the 200mV reduction, about 40 meV is associated with the ligand effect and 130 to 200 meV to the bifunctional mechanism. Thus, the bifunctional mechanism is approximately 4 times larger than the ligand effect for the enhancement of CO oxidation from the platinum catalyst.

Acknowledgment. This material is based upon work supported by the Department of Energy under Grant No. DEGF-02-99ER14993. P. Waszczuk acknowledges support by the Department of Energy Grant No. DOE LANL 30167010139. Any opinions, findings, and conclusions or recommendations expressed in this publication are those of the authors and do not necessarily reflect the views of The Department of Energy.

References and Notes

(1) Hamnett, A., Mechanism of Methanol Electro-Oxidation, in *Interfacial Electrochemistry: Theory, Experiment, and Applications*; Wieckowski, A. Ed.; Marcel Dekker: New York, 1999; 843−884.

(2) Watanabe, M.; Motoo, S. *J. Electroanal. Chem.* **1975**, *60*, 283.

(3) Ticanelli, E.; Beery, J. G.; Paffett, M. T.; Gottesfeld, S. *J. Electroanal. Chem.* **1989**, *258*, 61.

(4) Tremiliosi, G.; Kim, H.; Chrzanowski, W.; Wieckowski, A.; Grzybowska, B.; Kulesza, P. *J. Electroanal. Chem.* **1999**, *467*, 143.

(5) Davies, J. C.; Hayden, B. E.; Pegg, D. J. *Surf. Sci.* **2000**, *467*, 118.

(6) Goodenough, J. B.; Hamnett, A.; Manoharan, R.; Kennedy, B. J.; Weeks, S. A. *J. Electroanal. Chem.* **1988**, *240*, 133.

(7) Iwasita, T.; Nart, F. C.; Vielstich, W. *Ber. Bunsenegs. Phys. Chem.* **1990**, *94*, 1030.

(8) Krausa, M.; Vielstich, W. *J. Electroanal. Chem.* **1994**, *379*, 307.

(9) Frelink, T.; Visscher, W.; Vanveen, J. A. R. *Surf. Sci.* **1995**, *335*, 353.

(10) Frelink, T., W. Visscher, and J. A. R. Vanveen, Langmuir, **1996**, *12*, 3702.

(11) Hadzi-Jordanov, S.; Angerstein-Kozlowska, H.; Vukovic, M.; Conway, B. E.; *J. Phys. Chem.* **1977**, *81*, 2271.

(12) Gasteiger, H. A.; Markovic, N.; Ross, P. N.; Cairns, E. J. *J. Phys. Chem.* **1993**, *97*, 12 020.

(13) Tong, Y. Y.; Kim, H. S.; Babu, P. K.; Waszczuk, P.; Wieckowski, A.; Oldfield, E. *J. Am. Chem. Soc.* **2002**, *124*, 468.

(14) Wang, J.; Masel, R. I. *J. Am. Chem. Soc.* **199**, *113*, 5850.

(15) Wang, J.; Masel, R. I. *Surf. Sci.* **1991**, *243*, 199.

(16) Wang, J.; Masel, R. I. *J. Catal.* **1991**, *126*, 519.

(17) Lu, C.; Masel, R. I. *J. Phys. Chem. B* **2001**, *105*, 9793.

(18) Chrzanowski, W.; Wieckowski, A. *Langmuir* **1997**,*13*, 5974.

(19) Crown, A.; Wieckowski, A. *Phys. Chem. Chem. Phys.* **2001**, *3*, 3290.

(20) Tong, Y. Y.; Rice, C.; Godbout, N.; Wieckowski, A.; Oldfield, E. *J. Am. Chem. Soc.* **1999**, *121*, 2996.

(21) Waszczuk, P.; Wieckowski, A.; Zelenay, P.; Gottesfeld, S.; Coutanceau, C.; Leger, J. M.; Lamy, C.; *J. Electroanal. Chem.* **2001**, *511*, 55.

(22) Waszczuk, P.; Solla-Gullon, J.; Kim, H. S.; Tong, Y. Y.; Montiel, V.; Aldaz, A.; Wieckowski, A. *J. Catal.* **2001**, *203*, 1.

(23) Bendorf, C.; Nobl, C.; Madey, T. E. *Surf. Sci.* **1984**, *138*, 292.

(24) Capitano, A. T.; Gabelnick, A. M.; Gland, J. L. *Surf. Sci.* **1999**, *419*, 104.

(25) Koper, M. T. M.; Lukkien, J. J.; Jansen, A. P. J.; van Santen, R. A.; *J. Phys. Chem. B* **1999**, *103*, 5522.

(26) Pedersen, M. O.; Helveg, S.; Ruban, A.; Stensgaard, I.; Laegsgaard, E.; Norksov, J. K.; Besenbacher, F. *Surf. Sci.* **1999**, *426*, 395.

(27) Masel, R. I. *Chemical Kinetics and Catalysis*; Wiley: New York, 2001.

(28) McBreen, J.; Mukerjee, S. In *Interfacial Electrochemistry: Theory, Experiment, and Applications*; Wieckowski, A., Ed.; Marcel Dekker: New York, 1999, p 895.